PROCEEDINGS, 44th Workshop on Geothermal Reservoir Engineering
Stanford University, Stanford, California, February 11-13, 2019
SGP-TR-214

Numerical Study on Effects of Hydraulic Fracture Geometries on Heat Extraction Performance of a Multilateral-well Enhanced Geothermal System

Yu Shi, Xianzhi Song *, Gaosheng Wang, Jiacheng Li, Feixue YuLong

State Key Laboratory of Petroleum Resources and Prospecting, China University of Petroleum, Beijing, Beijing 102249, China

yushicupb@gmail.com, songxz@cup.edu.cn, 1968068343@qq.com, 371179440@qq.com, 275783350@qq.com

Keywords: Geothermal energy; enhanced geothermal system; hydraulic fracture; heat extraction performance; multilateral wells

ABSTRACT

Our previous study (Song et al, 2018) proposed a novel enhanced geothermal system (EGS) with multilateral wells and demonstrated that it had greater heat extraction performance than double-well EGS. However, hydraulic fracturing plays an extremely important role in improving the heat extraction performance of multilateral-well EGS. Therefore, it is significant to investigate effects of hydraulic fracture geometries on the multilateral-well EGS performance. In this study, we use a thermal-hydraulic-mechanical (THM) coupling model to find that which kind of fracture network geometry is suitable for improving multilateral-well EGS performance. Based on the model, effects of hydraulic fracture stages and hydraulic fracture complexities on the multilateral-well EGS performance are investigated. The results indicate that the increase of the hydraulic fracture stages could reduce the injection pressure and facilitate the thermal breakthrough. The hydraulic fractures with longer fractures and without too many direct connections between lateral wells and fractures is beneficial for the improvement of multilateral-well EGS performance. The results of this study provide significant suggestions for the fracturing operation of multilateral-well EGS.

1. INTRODUCTION

Geothermal energy is a popular renewable, sustainable and environmentally friendly natural resource. The enhanced geothermal system (EGS) is especially proposed to exploit high temperature geothermal energy, such as hot dry rock, for electricity generation (Tester et al, 2007). Our previous study (Song et al, 2018; Shi et al, 2018) proposed a novel multilateral-well EGS to simultaneously achieve injection and production through one main wellbore, which is shown in Figure 1. For this EGS, upper injection lateral wells and lower production lateral wells are sidetracked from the main wellbore. Next, a central tube with a heat insulation structure is installed in the wellbore and the annulus is sealed by packers. The working fluid is injected from the annulus and injection lateral wells. After the working fluid extracts heat from the geothermal reservoir, it is produced from production lateral wells and the central tube.

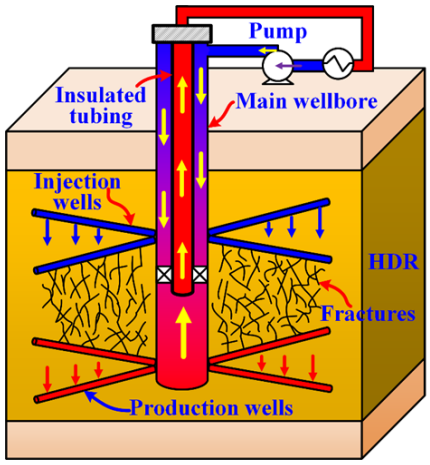

Figure 1: Schematic diagram of heat extraction of multilateral-well EGS (Song et al, 2018)

For multilateral-well EGS, reservoir stimulation is necessary to create fracture network to enhance the reservoir permeability and to provide heat transfer channels for the working fluid (Tester et al, 2007). Through fracturing operation, complex hydraulic fracture networks can be generated (Maxwell et al, 2002; Cipolla et al, 2010; Yang et al, 2017; Zhang et al, 2018). Therefore, it is very significant to study the heat extraction performances of multilateral-well EGS under various hydraulic fracture geometries, which will provide great suggestions about creating which kind of fractures through fracturing operation of multilateral-well EGS.

There are many numerical studies conducted on heat extraction performances of geothermal reservoir with discrete fracture network. For example, Fu et al. (2016) used a 2D numerical model to study the effects of fracture length, orientation and connectivity on EGS performance based on a random discrete fracture network. Chen et al. (2018) utilized a unified pipe-network model to investigate the

effects of fracture aperture on temperature distribution based on a randomly distributed fracture network. Sun et al. (2017) and Yao et al. (2018) conducted the sensitivity analysis of EGS performance through 2D and 3D THM coupling models with a discrete fracture network, respectively. However, above studies just focused on a single fracture network geometry and few studies investigated the effects of complex fracture networks on EGS performance.

This paper uses a 3D THM coupling model to study the effects of hydraulic fracture stage quantity on multilateral-well EGS performance. Based on the model, the heat extraction performances of three kinds of complex hydraulic fracture network geometries are compared for the multilateral-well EGS. The simulation results provide significant suggestions on fracturing operation of the multilateral-well EGS.

2. MODEL DEVELOPMENT

2.1 Model assumptions

In this paper, supercritical CO_2 is considered as the working fluid of the multilateral-well EGS, because CO_2 is a favorable working fluid for heat and mass transfer (Brown, 2000; Pruess, 2006; Pruess, 2008). Generally, under the multilateral-well EGS operation conditions, the temperature and pressure are always above 7.38 MPa and 31.1 ºC, respectively, so CO_2 is in a supercritical state in the multilateral-well EGS. To accurately calculate CO_2 properties, the equation of state for CO_2 proposed by Span and Wagner (S-W EOS) (Span and Wagner, 1996) is utilized to obtain CO_2 density and heat capacity, while the viscosity and thermal conductivity of CO_2 are explicitly calculated by equations in the references (Heidaryan et al, 2011; Jarrahian and Heidaryan, 2012). This is because these equations have a high accuracy in a wide applicable range. Besides, we assume that the fluid flow in the matrix and fractures is in laminar regime and can be described by Darcy's Law and that the reservoir rock is homogeneous and isotropic.

2.2 Mathematical equations

The fluid flow in the rock matrix fractures is described by the poroelastic storage model.

$$\rho_f S \frac{\partial p}{\partial t} - \nabla \cdot \rho_f \left[\frac{k}{\eta_f} \left(\nabla p + \rho_f g \nabla z \right) \right] = -\rho_f \alpha_B \frac{\partial e}{\partial t} - Q_f \tag{1}$$

$$d_f \rho_f S \frac{\partial p}{\partial t} - \nabla_\tau \cdot d_f \rho_f \left[\frac{k_f}{\eta_f} \left(\nabla_\tau p + \rho_f g \nabla_\tau z \right) \right] = -d_f \rho_f \alpha_B \frac{\partial e}{\partial t} + d_f Q_f \tag{2}$$

where ρ_f (kg/m^3) and p (Pa) are the fluid density and the pore pressure, respectively. t (s) is time and η_f (Pa·s) is the fluid viscosity. The parameter g (m/s^2) indicates the gravity acceleration. k and k_f (m^2) represent the rock matrix permeability and fracture permeability, respectively. d_f (m) is the fracture aperture. e denotes the volumetric strain caused by the rock deformation, which is determined by the equilibrium equation. The parameter Q_f represents the mass transfer between the rock matrix and fractures. α_B is Biot-Willis coefficient.

The heat transfer in the geothermal reservoir and fractures is described by the local thermal equilibrium model. Therefore, the energy conservation equations in the reservoir matrix and fractures are expressed as

$$\left(\rho c_p \right)_{eff} \frac{\partial T}{\partial t} + \rho_f c_{p,f} V \cdot \nabla T - \nabla \cdot \left(\lambda_{eff} \nabla T \right) = -Q_{f,E} \tag{3}$$

$$d_f \left(\rho c_p \right)_{eff} \frac{\partial T}{\partial t} + d_f \rho_f c_{p,f} V_f \cdot \nabla_\tau T - \nabla_\tau \cdot \left(d_f \lambda_{eff} \nabla T \right) = d_f Q_{f,E} \tag{4}$$

where the parameters T (K) and $c_{p,f}$ (J/(kg·K)) represent the reservoir temperature and the heat capacity of the working fluid. The parameter V (m/s) is the fluid velocity. The parameter $Q_{f,E}$ indicates the heat transfer between the reservoir matrix and fractures. $(\rho_{cp})_{eff}$ and λ_{eff} are the effective volumetric capacity and the effective thermal conductivity, respectively, which are calculated by

$$\left(\rho c_p \right)_{eff} = \left(1 - \varphi \right) \rho_s c_{p,s} + \varphi \rho_f c_{p,f} \tag{5}$$

$$\lambda_{eff} = \left(1 - \varphi \right) \lambda_s + \varphi \lambda_f \tag{6}$$

where ρ_s (kg/m^3), $c_{p,s}$ (J/(kg·K)) and λ_s (W/(m·K)) represent the density, heat capacity and thermal conductivity of the solid part in the reservoir, respectively.

The heat extraction process in the geothermal reservoir can lead to temperature variations and induce thermal stress in the rock. The effective stress of the rock also can be altered by the variation of pore pressure. On the other side, the variation of effective stress results in the rock deformation, which can change the fracture permeability and has significant effects on the fluid flow and heat transfer of the working fluid. Therefore, the heat extraction of the multilateral-well EGS is a thermal-hydraulic-mechanical coupled process. The rock deformation is described by the equilibrium equation.

$$\mu u_{i,jj} + (\lambda + \mu) u_{j,ji} - \alpha_B p_{,i} - 3K_d \alpha_T \Delta T_{,i} + F_i = 0 \tag{7}$$

where u (m) represents the displacement. λ (Pa) and μ (Pa) are Lamé parameters and expressed by elastic modulus E (Pa) and poisson's ratio v, i.e. $\lambda=Ev/[(1+v)(1-2v)]$, $\mu=E/[2(1+v)]$. The third term denotes the effect of pore pressure and the fourth term represents the thermal stress induced by the temperature variations. $\Delta T=T-T_i$, where T_i (K) represents the initial temperature of the reservoir. K_d (Pa) can be expressed as $K_d=E/[3(1-2v)]$. α_T (K^{-1}) is the coefficient of thermal expansion. F_i is the body force per unit volume in the i-coordinate.

The volumetric strain e in Eqs. (1) and (2) is related to the effective stress and formulated by

$$e = \left(\frac{\sigma_1 + \sigma_2 + \sigma_3}{3} + \alpha_B p \right) / K_d \tag{8}$$

where σ_1, σ_2 and σ_3 represent the primary, secondary and third principal stresses. In this model, we assume that the tensile stress is positive and compressive stress is negative.

The fracture permeability evolution is related to the normal effective stress and the relationship can be expressed as (Miller, 2015)

$$k_f = k_0 e^{-(\sigma_n'/\sigma^*)} \tag{9}$$

where k_0 (m^2) is the initial permeability when $\sigma'_n=0$. σ^* is a normalizing constant and set as -10 MPa (Sun et al, 2018; Yao et al, 2018; Miller, 2015) in this paper. σ'_n is the effective normal stress imposed on the fracture plane and is expressed by

$$\sigma_n' = K_n \left(u_n - d_f \alpha_T \Delta T \right) \tag{10}$$

where u_n (m) is the normal displacement of fractures. K_n (Pa/m) is the stiffness of fractures and considered as 400 Gpa/m in this paper (sun et al, 2017; Yao et al, 2018).

3. A MULTILATERAL-WELL EGS WITH HYDRAULIC FRACTURES

3.1 Computational model

The above mathematical equations are solved by the finite element solver COMSOL. Figure 2 illustrates the schematic of the computational model for a multilateral-well EGS with a three stages of hydraulic fracture network. The model includes an enclosing rock, the fractured reservoir with primary and secondary hydraulic fractures, 4 upper injection lateral wells and 4 lower production lateral wells. The fracture width for the primary and secondary fractures is 0.5 mm. The fracture conductivities of the primary and secondary fractures are 25 md·m and 5 md·m, respectively. The enclosing rock is a 1000 m × 1000 m × 1000 m cube, which is located at a depth from 3000 m to 4000 m. The fractured reservoir with a size of 500 m × 500 m × 500 m is located at the center of the enclosing rock. The vertical distance between the upper injection and lower production lateral wells is 400 m. The length and diameter of lateral wells are 150 m and 0.10 m, respectively. The other physical properties of reservoir and fractures are listed in Table 1.

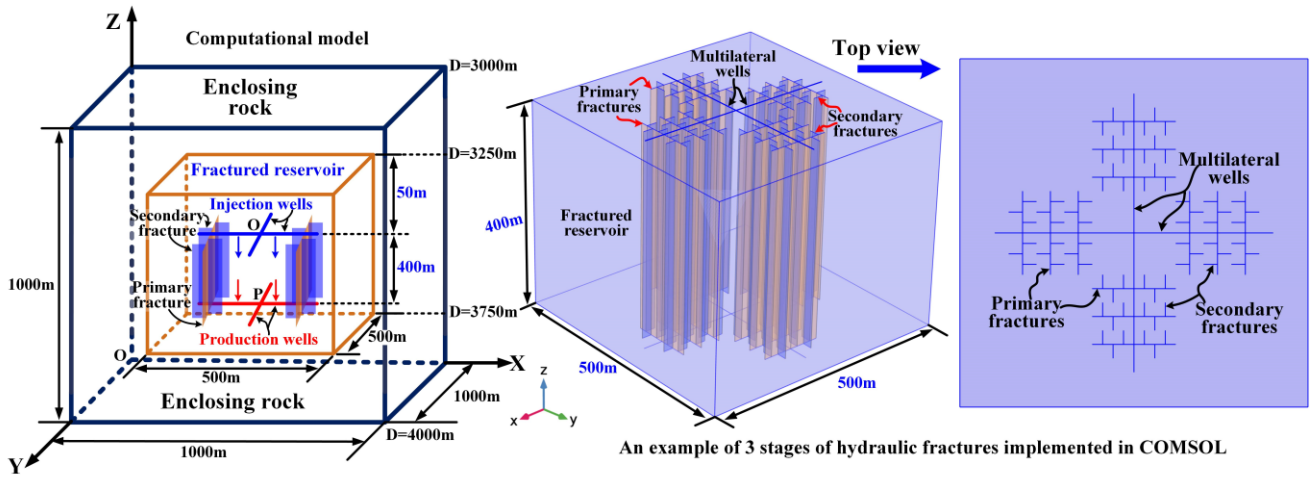

Figure 2: Schematic of the computational model

After the computational model in figure 2 is constructed in COMSOL, the domain is meshed with triangular prismatic elements. The meshes for the fractured reservoir are much finer than those for the enclosing rock, because the heat extraction process mainly happens in the fractured reservoir. In terms of computational efficiency and accuracy, the whole computational model has a mesh quantity of

120,000. Besides, COMSOL uses the segregated solution method to solve the THM coupling equations. The simulation time is 30 years and the time step is set as 1 day. The relative tolerance is 10^{-6} and considered as the convergence criteria.

Table 1: The reservoir and fracture properties

Items	Enclosing rock	Fractured reservoir matrix	Primary fractures	Secondary fractures
Density (kg/m^3)	2800	2700	2000	2000
Heat conductivity (W/(m·K))	3	2.8	2.8	2.8
Heat capacity (J/(kg·K))	1000	1000	850	850
Porosity (%)	1	5	100	100
Permeability (m^2)	10^{-18}	5×10^{-16}	5×10^{-11} (k_0)	10^{-11} (k_0)
α_T	5×10^{-6}	5×10^{-6}	5×10^{-6}	5×10^{-6}
Elastic modulus (Pa)	2.5×10^{10}	2.5×10^{10}	2.5×10^{10}	2.5×10^{10}
Poisson's ratio	0.25	0.25	0.25	0.25
α_B	0.7	0.7	0.7	0.7

3.2 Initial and boundary conditions

The initial reservoir temperature and pressure increase linearly from the top to bottom boundaries with the geothermal and pressure gradients of 0.05 K/m and 5000 Pa/m, respectively. The initial temperature and pressure on the top boundary are 473.15 K and 30 MPa, respectively. The top boundary is assumed to be insulated by the cap rock. The temperature at the bottom and side boundaries remains constant at the initial reservoir temperature. The no-flow condition is exerted at all boundaries. Furthermore, the normal displacements of all boundaries are constrained. This is because we just focus on the stress evolution induced by variations of temperature and pore pressure during the heat extraction and the initial geo-stress is not taken into consideration (Sun et al, 2017; Yao et al, 2018). The injection temperature and mass flow rate of the working fluid for the injection lateral wells remain at 333.15 K and 50 kg/s, respectively. The pressure of production lateral wells is set as 25 MPa.

3.3 Hydraulic fracture network geometries

The 6 different hydraulic fracture network geometries are shown in figure 3. Figure 3 just shows the top views of the hydraulic fracture network geometries. In the figure, the blue lines represent lateral wells, while the yellow and green lines indicate the primary and secondary fractures. The symbol *d* in Case 1 means the distance between the first stage hydraulic fracture and the central of lateral wells. *d* is set as 80 m in the model. The distance between two adjacent primary fractures is 40 m. For Cases 1, 2 and 3, the half-length of primary fracture is 60 m and the secondary fracture length is 20 m. The heat extraction performances of these three cases are compared to study the effects of primary fracture stage quantity on multilateral-well EGS performance. For Case 4, each secondary fracture is connected with another secondary fracture and the fracture length is 20 m. For Case 5, there are 6 long secondary fractures orthogonally connected with the primary fracture and the secondary fracture length is 120 m. For Case 6, there are two sets of secondary fractures. One set of secondary fracture is orthogonally connected with primary fractures, while another set is perpendicular to the lateral wells. The lengths of these two sets of secondary fractures are 120 m and 110 m, respectively. The heat extraction performances of Cases 3, 4, 5 and 6 are compared to investigate the effects of hydraulic fracture complexity on multilateral-well EGS performance.

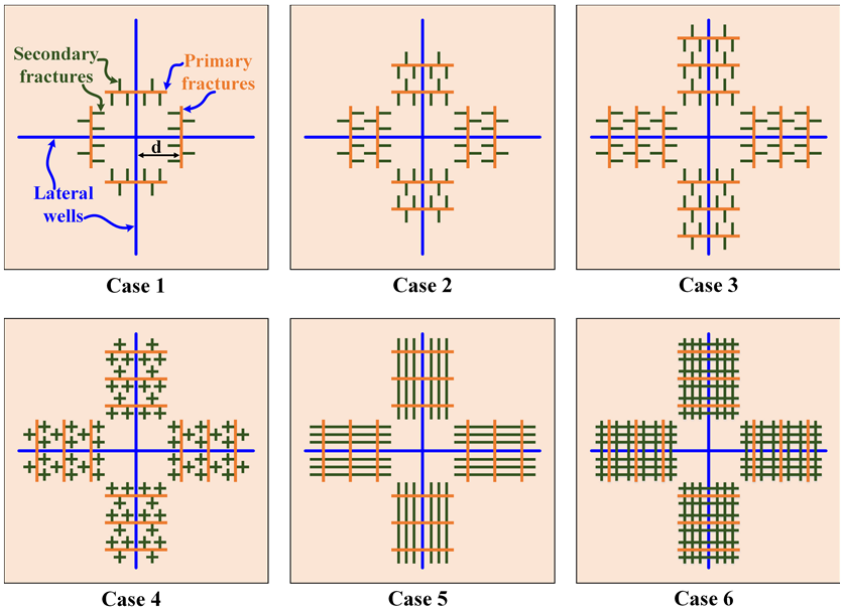

Figure 3: Top views of various complex fracture network geometries

4. SIMULATION RESULTS

4.1 Effects of hydraulic fracture stage quantity

In this section, the effects of the primary fracture stage quantity on the multilateral-well EGS performance are studied through Cases 1, 2 and 3. The temperature contours on different cross sections of the fractured reservoir with various primary fracture stages after 30 years are illustrated in figure 4. The schematic of the cross sections are shown in figure 5. The *xz* section at *y*=500 m indicates the middle *xz* plane of the fractured reservoir. The *xy* section at *z*=300 m represents the plane where production lateral wells are located, while the *xy* section at *z*=700 m indicates the plane where injection lateral wells are located. To facilitate the expression, the xz section at *y*=500 m, *xy* section at *z*=300 m and *xy* section at *z*=700 m are named as section 1, section 2 and section 3, respectively. Besides, it is worth noting that the mentioned cross sections in the following studies are the same as those marked in figure 5.

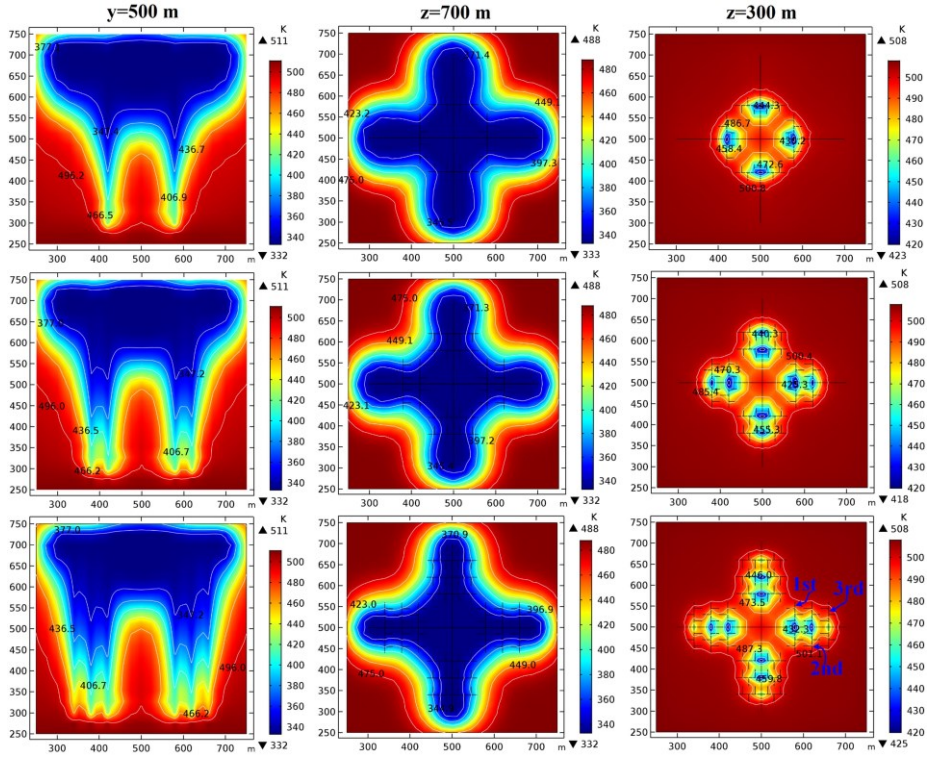

Figure 4: Temperature contours on different cross sections of fractured reservoir with various primary fracture stages after 30 years (first row: Case 1, second row: Case 2, third row: Case 3)

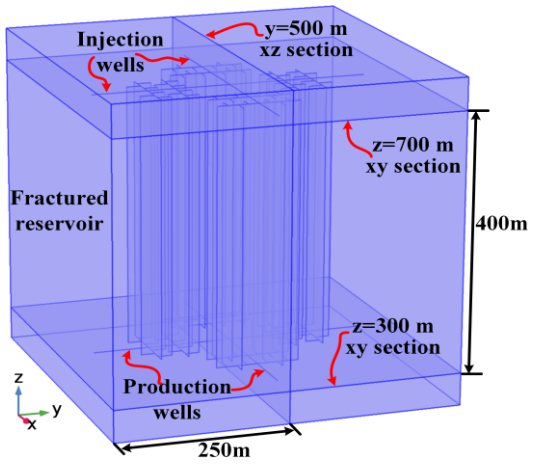

Figure 5: Schematic of different cross sections of the fractured reservoir in computational domain

The white lines in figure 4 represent the isotherms. We can see from the section 1 that as the primary fracture stage quantity increases, the cooling area along the vertical direction expands and the number of preferential channel improves. It means that with the increase of fracture stage, the cooling working fluid tends to break through along the vertical fractures rather than dispersing along the horizontal

section. This can be also founded from section 2. The cooling area along the horizontal section decreases when there are more primary fractures. Another significant finding is that the minimum temperature on the section 3 for three primary fracture stages is 425 K, higher than those for one and two primary fracture stages. This is because that as the primary fracture stage quantity increases, most injected working fluid flows to the production lateral wells through fractures rather than rock matrix. However, when there are three primary fracture stages, the working fluid can be scattered by more preferential channels, which decreases the flow rate of working fluid in the first stage primary fracture. Nevertheless, the total cooling area on the section 3 for Case 3 is the largest among these three cases, although its minimum temperature shows the highest value. Furthermore, we can also see from the section 3 for Case 3 that the temperature around the third stage fracture is higher than those around the first and second stage fracture, which means that the flow rate in the first and second stage fracture is higher than that in the third stage fracture. This phenomenon is induced by the pressure loss along the lateral wells.

The average production temperatures and injection pressures under various primary fracture stages are shown in figure 6, while the output thermal power of these three cases is plotted in figure 7. It can be concluded that as the quantity of primary fracture stage increases, the average production temperature and output thermal power decrease dramatically more than 10 K and 0.69 MW from Case 1 to Case 3 after 30 years, respectively, while the injectivity of multilateral-well EGS is improved obviously. The results coincide well with the temperature contours shown in figure 4. Furthermore, comparing Case 2 to Case 3, we can see that the production temperature of three fracture stages is just about 2 K less than that of two fracture stages, while the injection pressure can be decreased 3 MPa. Therefore, it suggests that in terms of great injectivity and proper production temperature, three primary fracture stages may be more appropriate for the multilateral-well EGS.

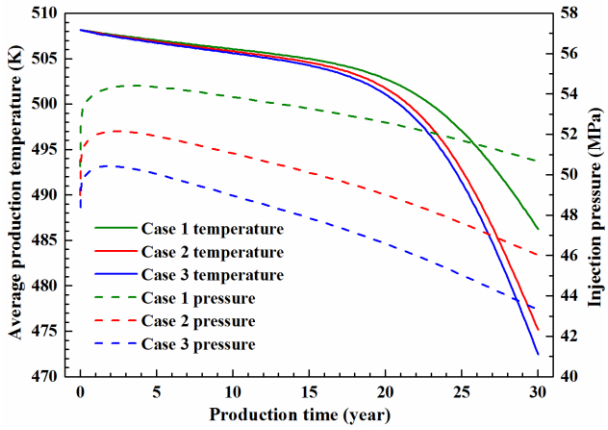

Figure 6: Average production temperatures and injection pressures under various primary fracture stages

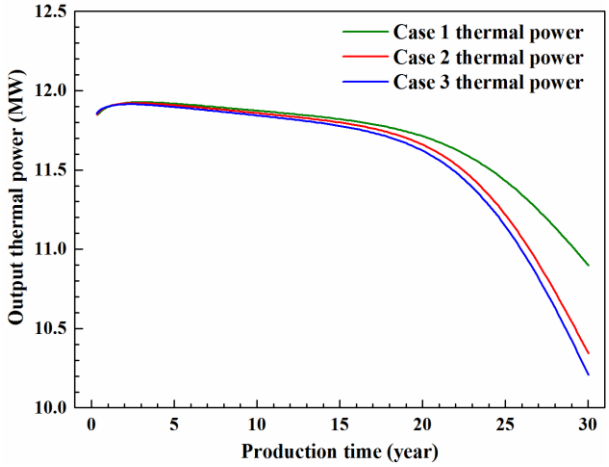

Figure 7: Output thermal power under various primary fracture stages

4.2 Effects of hydraulic fracture complexity

Generally, the fracture network generated by fracturing operation has complex geometries. In this section, the effects of fracture complexity on heat extraction performance of multilateral-well EGS are investigated through Cases 3, 4, 5 and 6. The temperature contours on different cross sections of fractured reservoir with various fracture complexities after 30 years are demonstrated in figure 8. We can see that the cooling areas on the section 1 and section 2 of these three cases are similar to each other. It indicates that for the three cases, the heat extraction process mainly happens around the fracture network. However, the thermal breakthrough on the section

3 of Case 6 is much more obvious than that of Case 4 and Case 5, and the total cooling areas of Case 6 is the largest among these three cases. Furthermore, the minimum temperature of Case 6 is 401 K, much lower than those of Case 4 and Case 5. This is because that there are additional secondary fractures to directly connect the injection and production lateral wells, which provides many preferential channels for the working fluid and promotes the thermal breakthrough. For Cases 4 and 5, the total secondary fracture length are the same. However, the length of each secondary fracture is shorter and the secondary fracture quantity is higher for Case 4. Comparing temperature contours on section 3 of Cases 4 and 5, we can find that the thermal breakthrough of Case 4 is more obvious than that of Case 5. The cooling region of Case 4 is restricted around the lateral wells, which means that the heat extraction concentrates in the fractures near the lateral wells. In contrast, the minimum temperature is higher and the influence area of heat extraction is larger for Case 5, which indicates that the working fluid can be dispersed farther away from the lateral wells.

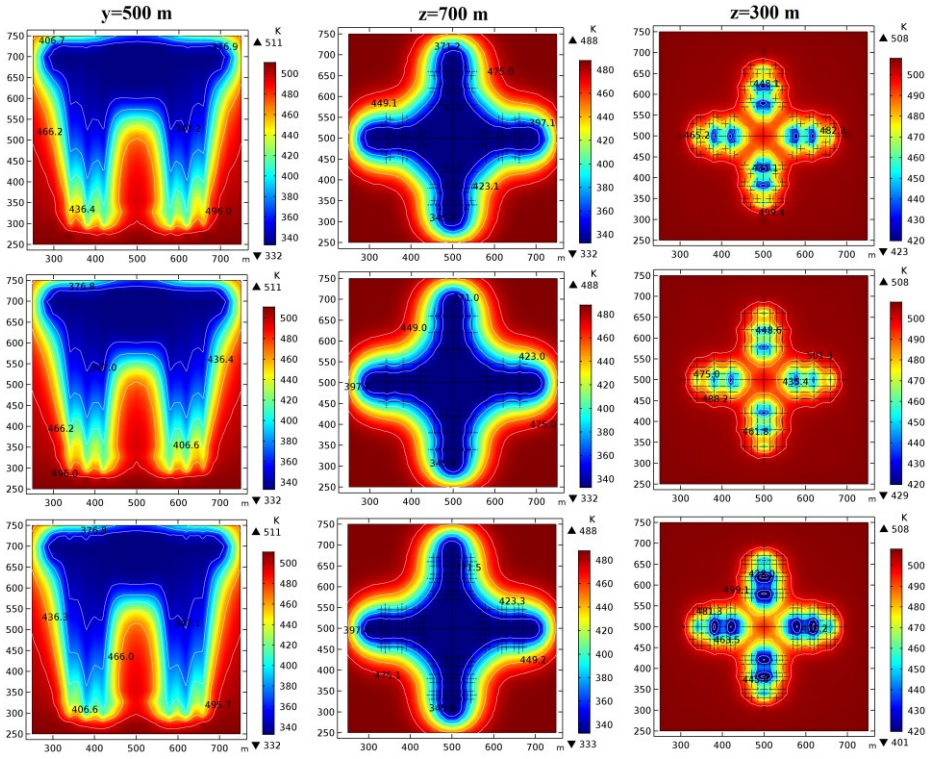

Figure 8: Temperature contours on different cross sections of fractured reservoir with various fracture complexities after 30 years (first row: Case 4, second row: Case 5, third row: Case 6)

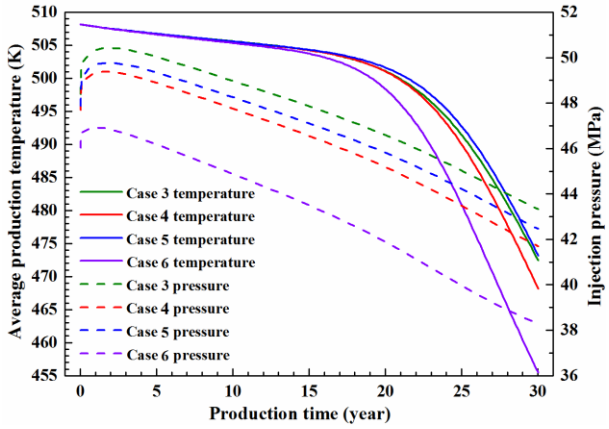

Figure 9: Average production temperatures and injection pressures under various hydraulic fracture complexities

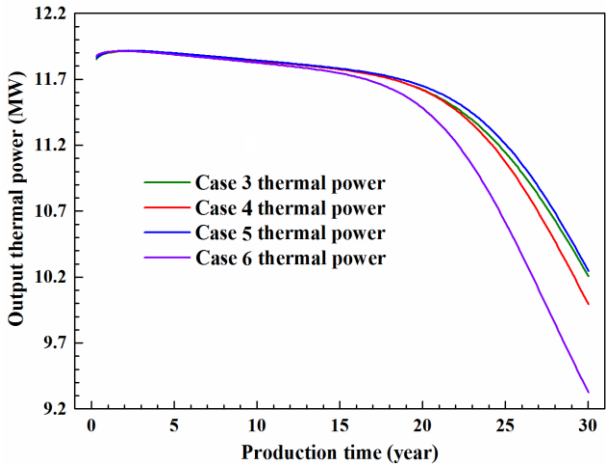

Figure 10: Output thermal power under various hydraulic fracture complexities

Figure 9 and figure 10 illustrate the average production temperatures, injection pressures and output thermal power under various hydraulic fracture complexities, respectively. We can see that the production temperature, output thermal power and injection pressure of Case 6 show the lowest value among the four cases. It demonstrates that more fractures indeed improve the injectivity dramatically, but only increasing the fracture quantity connected with lateral wells could accelerate production temperature drawdown. Comparing Case 3 and Case 5, the production temperature and thermal power of Case 5 is higher, while its injection pressure is lower. It indicates that increasing fracture length is beneficial for improving the multilateral-well EGS efficiency. However, if the quantity of secondary fracture around the lateral wells increases, the production temperature and thermal power decline (seen from Case 4). It suggests that increasing the fracture length is an efficient way to enhance the connection between fractures and reservoir rock and to improve the heat extraction performance of multilateral-well EGS.

5. CONCLUSIONS

This paper uses a 3D THM coupling model to study the effects of hydraulic fracture network on the heat extraction performance of multilateral-well EGS. The influence of the primary hydraulic fracture stage quantity on the multilateral-well EGS performance is investigated. The heat extraction performances of various hydraulic fracture network complexities are compared. There are two key findings obtained from the simulation results.

The quantity of primary fracture stage has significant effects on the multilateral-well EGS performance. With the increase of primary fracture stage, the production temperature and thermal power of multilateral-well EGS decrease, while the injectivity is improved. It indicates that more primary fractures provide more preferential channels to connect injection and production wells and promote the thermal breakthrough. In terms of lower injection pressure and proper production temperature, it suggests that 3 stages of primary fractures are appropriate for multilateral-well EGS.

It suggests that the fracturing operation of multilateral-well EGS should focus on creating long secondary fractures to connect a large area of reservoir rock, rather than generating many primary fractures around lateral wells.

ACKNOWLEDGEMENTS

The authors would like to acknowledge the National Natural Science Funds for Excellent Young Scholars of China (Grant No. 51822406) and National Key Research and Development Program of China (Grant No. 2016YFE0124600). Besides, support from the Program of Introducing Talents of Discipline to Chinese Universities (111 Plan) (Grant NO. B17045) is appreciated.

REFERENCES

Brown, D.W.: A hot dry rock geothermal energy concept utilizing supercritical CO_2 instead of water, *Proceedings,* 25th Workshop on Geothermal Reservoir Engineering, Stanford University, Stanford, CA (2000).

Chen, Y., Ma, G., Wang, H., and Li, T.: Evaluation of geothermal development in fractured hot dry rock based on three dimensional unified pipe-network method, *Applied Thermal Engineering*, **136**, (2018), 219-28.

Cipolla, C.L., Warpinski, N.R., Mayerhofer, M., Lolon, E.P., and Vincent, M.: The relationship between fracture complexity, reservoir properties, and fracture-treatment design, *SPE production & Operations*, **25**, (2010), 438-52.

Fu, P., Hao, Y., Walsh, S.D.C., and Carrigan, C.R.: Thermal drawdown-induced flow channeling in fractured geothermal reservoirs, *Rock Mechanics and Rock Engineering*, **49**, (2016), 1001-24.

Heidaryan, E., Hatami, T., Rahimi, M., and Moghadasi, J.: Viscosity of pure carbon dioxide at supercritical region: Measurement and correlation approach, *The Journal of Supercritical Fluids*, **56**, (2011), 144-51.

Jarrahian, A., and Heidaryan, E.: A novel correlation approach to estimate thermal conductivity of pure carbon dioxide in the supercritical region, *The Journal of Supercritical Fluids*, **64**, (2012), 39-45.

Maxwell, S.C., Urbancic, T.I., Steinsberger, N., and Zinno, R.: Microseismic imaging of hydraulic fracture complexity in the Barnett shale, *SPE Annual Technical Conference and Exhibition*, San Antonio, Texas (2002).

Miller, S.A.: Modeling enhanced geothermal systems and the essential nature of large scale changes in permeability at the onset of slip, *Geofluids*, **15**, (2015), 338-49.

Pruess, K.: Enhanced geothermal systems (EGS) using CO_2 as working fluid—A novel approach for generating renewable energy with simultaneous sequestration of carbon, *Geothermics*, **35**, (2006), 351-67.

Pruess, K.: On production behavior of enhanced geothermal systems with CO_2 as working fluid, *Energy Conversion and Management*, **49**, (2008), 1446-54.

Shi, Y., Song, X., Shen, Z., Wang, G., Li, X., and Zheng, R.: Numerical investigation on heat extraction performance of a CO_2 enhanced geothermal system with multilateral wells, *Energy*, **163**, (2018), 38-51.

Song, X., Shi, Y., Li, G., Yang, R., Wang, G., Zheng, R.: Numerical simulation of heat extraction performance in enhanced geothermal system with multilateral wells, *Applied Energy*, **218**, (2018), 325-37.

Span, R., Wagner, W.: A new equation of state for carbon dioxide covering the fluid region from the triple point temperature to 1100 K at pressures up to 800 MPa, *Journal of physical and chemical reference data*, **25**, (1996), 1509-96.

Sun, Z.X., Zhang, X., Xu, Y., Yao, J., Wang, H.X., and Lv, S.: Numerical simulation of the heat extraction in EGS with thermal-hydraulic-mechanical coupling method based on discrete fractures model, *Energy*, **120**, (2017), 20-33.

Tester, J.W., Anderson, B.J., Batchelor, A.S., Blackwell, D.D., DiPippo, R., Drake, E.M.: Impact of enhanced geothermal systems on US energy supply in the twenty first century, *Philosophical Transactions of the Royal Society of London A: Mathematical, Physical and Engineering Sciences*, **365**, (2007), 1057-94.

Yang, R., Huang, Z., Li, G., Yu, W., Sepehrnoori, K., Lashgari, H.R.: A Semianalytical Approach to Model Two-Phase Flowback of Shale-Gas Wells with Complex-Fracture-Network Geometries, *SPE Journal*, **22**, (2017), 1808-1833.

Yao, J., Zhang, X., Sun, Z., Huang, Z., Liu, J., Li, Y.: Numerical simulation of the heat extraction in 3D EGS with thermal-hydraulic-mechanical coupling method based on discrete fractures model, *Geothermics*, 74, (2018), 19-34.

Zhang, S., Huang, Z., Huang, P., Wu, X., Xiong, C., and Zhang, C.: Numerical and experimental analysis of hot dry rock fracturing stimulation with high-pressure abrasive liquid nitrogen jet, *Journal of Petroleum Science and Engineering*, **163**, (2018), 156-65.